이상 탐지를 이용하여 금성의 UVI 및 LIR 이미지를 사용하여 정지 대기파 탐지

Detecting Stationary Atmospheric Waves in Venus with a Self-Supervised Adversarial Model Using Anomaly Detection

요 약

Atmospheric waves on Venus are formed due to temperature changes, pressure, and other atmospheric variables propagating through the atmosphere. These patterns and oscillations may provide valuable insights into the planet's atmospheric dynamics and further characterization of the phenomenon. In this paper, we approach the detection of these atmospheric waves through an adversarially trained self-supervised anomaly detection model. We investigate two types of imaging: longwave infrared (LIR) and ultraviolet imaging (UVI). Distinct characteristics of LIR and UVI data present new opportunities to analyze the phenomenon and compare the machine learning performance. The results show that the model can differentiate between stationary waves and cloud formations, with an AUC score of 86.53% for LIR images and 90.81% for UVI images. Moreover, anomaly scores show UVI data is much less prone to mislabeling for normal cloud formations and stationary waves.

1. Introduction

Venus is the second planet from the Sun, similar in size and bulk chemical composition to Earth. However, its atmosphere is drastically different from that of Earth [7], mainly comprising CO_2 (carbon dioxide) and other minor compounds like SO_2 (sulfur dioxide), which can condense to form clouds at approximately 48-70 km of altitude [8].

Surface-level atmospheric waves on Venus, particularly stationary waves, result from a multitude of factors inherent to the dynamical processes of Venus' atmospheric phenomena. Such observational data of these waves yield profound insights into the intrinsic origins and dynamics of Venus' atmosphere. Specifically, stationary waves, characterized by their geographic persistence over extended temporal spans, serve as crucial indicators that hint at the potential correlations between atmospheric dynamics and corresponding topographical features on Venus' surface.

Historically, the identification and analysis of these stationary waves have been predominantly reliant on manual inspection conducted by experts. However, this methodology has become increasingly impractical, given the sporadic nature of these waves in existing datasets coupled with the increasing volume of data emanating from current missions, such as the ongoing Akatsuki space probe mission. When it comes to large datasets in a variety of domains, such manual approaches are not only time-consuming but also may lead to human errors and potential oversight of crucial data. With the advance of machine learning methodologies, task-specific designed models may outperform human experts [9, 3].

In response to these challenges, we implement a vector-quantized generative adversarial network (VQ-GAN) [10], a state-of-the-art generative model that builds upon our preceding investigation utilizing data collated by the longwave infrared (LIR) camera aboard the Akatsuki space probe. This research extends the scope of our dataset to encompass images captured by the Ultraviolet Imager (UVI) onboard the same spacecraft. Preliminary results indicate that our proposed model, when applied to the preprocessed data, exhibits superior performance in discriminating between images that either contain or lack stationary wave features, as compared to the results derived from our research focused on LIR data.

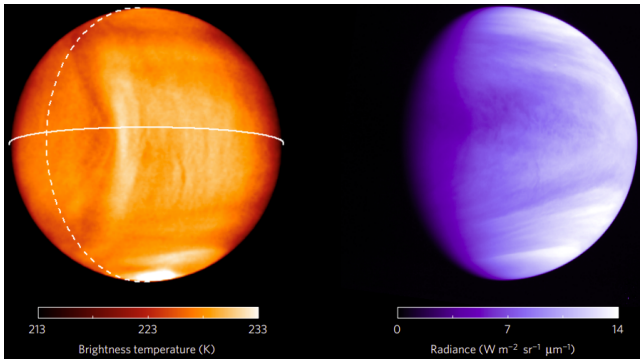

그림 1: LIR (on the left) and UVI (on the right) images of Venus, taken by the Akatsuki space probe on December 7, 2015 [4]

2. Experimental Settings

2.1 Dataset and Image Preprocessing

The LIR and UVI images taken by the Akatsuki probe provided by the Japan Aerospace Exploration Agency (JAXA), are publicly available.

UVI and LIR techniques present unique strengths and weaknesses. LIR uses a longwave infrared spectrum, which is associated with thermal emissions. This is useful for researching temperature mapping, penetration of cloud cover, and access to nightside imaging [2]. On the other hand, LIR may lack clarity and resolution, while indirect inference through temperature variations rather than direct observations may present contradicting information. UVI uses the ultraviolet part of the spectrum, ranging from 10nm to 400nm in wavelength. While UVI is useful for cloud pattern and structure research and SO2 detection , it has limited penetration into Venus' atmosphere due to thick clouds, which means it cannot provide surface details [1]. Data used in this study were taken by the Akatsuki Venus Orbiter in periods December 7th, 2015, and between March 2016 and January 2017, which are the same periods taken in a previous study with confirmed existence of stationary waves [5].

Both datasets consist of consecutive Venus images ranging from a few seconds to several hours. Due to the low-frequency nature of the features in each image, we performed multiple preprocessing

steps to highlight the features. The preprocessing pipeline starts with stacking images taken during the same orbiting period of the Akatsuki probe. As the stationary waves, as the name suggests, do not move relative to a sequence of relative consecutive images, the stationary waves are highlighted while the rest of the features are smoothed out.

We employed protocols for both image datasets to ensure the uniformity of output images. Specifically, the Brightness Temperature was normalized within the Longwave Infrared Radiation (LIR) dataset, facilitating a more homogenized set of output images. Concurrently, the Lambert Lommel-Seeliger Law (LLS) was applied to the Ultraviolet Imaging (UVI) dataset, effectively mitigating the impact of viewing geometry attributable to solar illumination [6]. This process resulted in output images characterized by uniform illumination, thereby removing inconsistencies that might arise due to irregular illumination patterns.

Additionally, we utilized a high-pass filtering technique to accentuate prominent features in the stacked UVI images. This process involved the utilization of a Gaussian-smoothed image, with a kernel size specified at (25,25), which subsequently yielded images where stationary waves were distinctly visible.

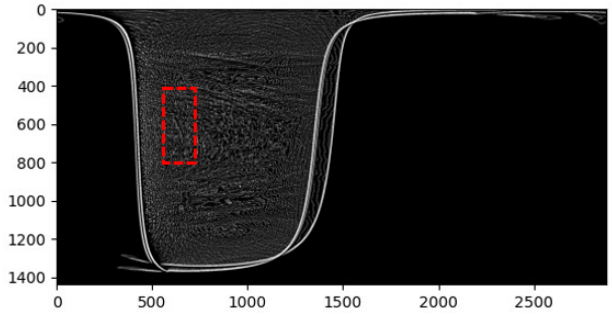

그림 2: UVI image after high-pass filtering taken during early an early period of December 2015.

In processing our model's image data, we divided each image into 72x72 pixel grids and excluded those with over 2500 black pixels for lacking sufficient information. This procedure yielded roughly 2000 normal and 50 stationary wave images in the UVI dataset. Similarly, the LIR dataset comprised around 600 normal and 60 stationary wave images.

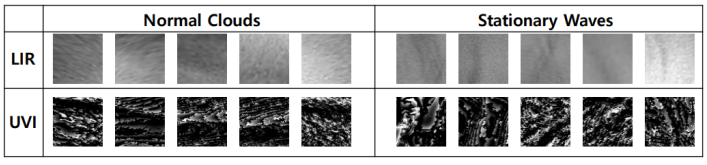

그림 3: Normal Cloud formation (on the left) and stationary wave feature comparison between the LIR and the UVI imaging methodologies.

2.2 Anomaly Detection Model

In this work, we use the VQ-GAN model. Different from other GANs, the generator uses a vector quantization layer to quantize the output into a discrete vector set, which affects the generator by forcing it to produce images that are similar to training data due to quantization ensuring that the generated images are a "nearest neighbor" of the training images in the discrete code space. For an input x that is encoded through an encoder E with a representation $E(x)$, there's a codebook C, which is a set of K codewords: $C = \{c_1, c_2, \ldots, c_K\}$. The goal of quantization is to find the closest codeword to the encoded representation $E(x)$, typically done using the Euclidean distance. Therefore, the quantized representation z_x becomes:

$$z_x = \arg\min_{c_i \in C} ||E(x) - c_i||_2. \tag{1}$$

The quantized latent representation is then propagated through the generator G to produce the reconstructed image $\tilde{x} = G(z_q)$. During the training, the discriminator D takes in the reconstructed and real images and classifies them as real or fake. Loss is given by:

$$L_D = -\left(\mathbb{E}[\log D(x)] + \mathbb{E}[\log(1 - D(\tilde{x}))]\right) \tag{2}$$

At the same time, G tries to generate better images through iterations, for which the loss function, mean squared error (MSE), is defined as:

$$L_{\text{MSE}} = \frac{1}{N}\sum_{i=1}^{N}(x_i - \tilde{x}_i)^2 \tag{3}$$

Using VQ-GAN for anomaly detection involves multiple steps. The reconstruction-based anomaly detection hypothesis dictates that if a model is trained with a particular class only, then the reconstruction of the class images should be successful in high and low dimensions. On the other hand, the model will fail to successfully reconstruct examples from a class that the model is not trained with. The discrepancy between the trained and untrained classes can be used for detecting anomaly-designated classes. Our experiment designates normal cloud formation patches as normal data and trains our model. We test the remaining normal cloud patches and the anomaly-designated stationary wave patches during the inference.

We compute the anomaly scores using high and low dimensions, for which the weighted anomaly scoring is shown below:

$$S = \lambda \times \text{L1}(x, \tilde{x}) + (1 - \lambda) \times \text{L2}(E(x), E(\tilde{x})) \tag{4}$$

where $\text{L1}(x, \tilde{x})$ is the L1 distance between the input and the reconstructed image, and $\text{L2}(E(x), E(\tilde{x}$ is the L2 distance between the latent representation of the input and the reconstructed image and λ is the weighting factor, in this experiment, taken as 0.8.

To make sure that the anomaly scores are on a comparable scale, we apply min-max normalization. Given a set of anomaly scores S_i for images $i = \{1, \ldots, N\}$, the normalized score S_i' is:

$$S_i' = \frac{S_i - \min(S)}{\max(S) - \min(S)} \tag{5}$$

We can then plot the anomaly distribution to observe the differences between the normal cloud formations and atmospheric stationary waves.

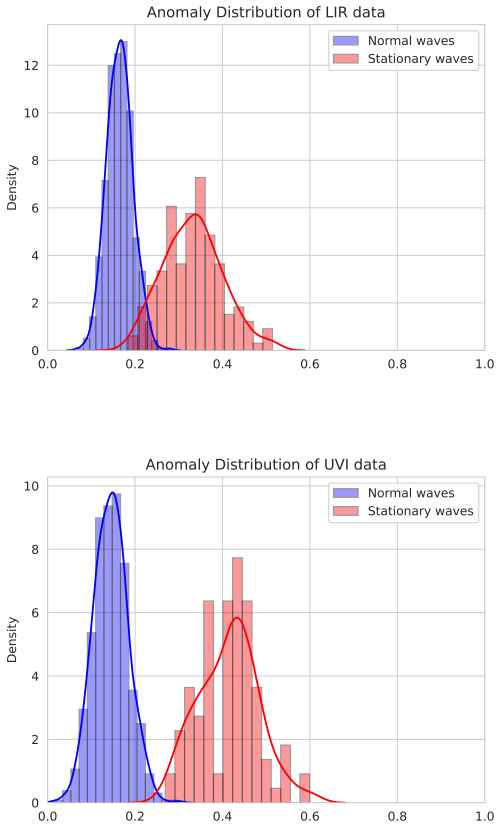

그림 4: Anomaly distributions between the LIR data (top) and the UVI data (bottom). It can be seen that anomaly scores for UVI data are higher than the LIR, and at the same time, anomaly scores for normal cloud formations are lower.

3. Experimental Analysis and Discussions

Although we observe that the UVI preprocessing step introduces a heavy amount of noise, it also makes it so that the stationary wave features are much more distinctive. On the contrary, LIR preprocessing causes a blurring effect on the image, making the stationary wave features harder to identify. This difference in feature quality is also reflected in our quantitative and qualitative analyses, where the model achieves 90.81% performance in AUC score using UVI data, compared to 86.53% AUC score using the LIR data. Anomaly detection distribution plots also highlight that the UVI data has much better normal data reconstruction quality and a higher overall anomaly detection rate than the LIR data.

4. Conclusion

In this work, we employed a self-supervised VQ-GAN for anomaly detection in atmospheric stationary waves and compared the efficacy of LIR and UVI datasets. Our quantitative and qualitative analyses revealed that the UVI dataset provides superior performance over the LIR dataset in anomaly detection. For future work, we aim to automate stationary feature detection and localization without using manual grid selection and change in the Venus atmosphere using temporal data.

참고 문헌

[1] *Venus II: Geology, Geophysics, Atmosphere, and Solar Wind Environment*. University of Arizona Press, 1997.

[2] Bruno Bézard, Catherine de Bergh, David Crisp, and Jean-Pierre Maillard. The deep atmosphere of venus revealed by high-resolution nightside spectra. *Nature*, 345(6275):508–511, Jun 1990.

[3] Samuel Dodge and Lina Karam. A study and comparison of human and deep learning recognition performance under visual distortions. In *2017 26th International Conference on Computer Communication and Networks (ICCCN)*, pages 1–7, 2017.

[4] Tetsuya Fukuhara, Masahiko Futaguchi, George L. Hashimoto, Takeshi Horinouchi, Takeshi Imamura, Naomoto Iwagaimi, Toru Kouyama, Shin-ya Murakami, Masato Nakamura, Kazunori Ogohara, Mitsuteru Sato, Takao M. Sato, Makoto Suzuki, Makoto Taguchi, Seiko Takagi, Munetaka Ueno, Shigeto Watanabe, Manabu Yamada, and Atsushi Yamazaki. Large stationary gravity wave in the atmosphere of venus. *Nature Geoscience*, 10(2):85–88, Feb 2017.

[5] Takehiko Kitahara, Takeshi Imamura, Takao M. Sato, Atsushi Yamazaki, Yeon Joo Lee, Manabu Yamada, Shigeto Watanabe, Makoto Taguchi, Tetsuya Fukuhara, Toru Kouyama, Shin-ya Murakami, George L. Hashimoto, Kazunori Ogohara, Hiroki Kashimura, Takeshi Horinouchi, and Masahiro Takagi. Stationary features at the cloud top of venus observed by ultraviolet imager onboard akatsuki. *Journal of Geophysical Research: Planets*, 124(5):1266–1281, 2019.

[6] Y.J. Lee, T. Imamura, S.E. Schröder, and E. Marcq. Long-term variations of the uv contrast on venus observed by the venus monitoring camera on board venus express. *Icarus*, 253:1–15, 2015.

[7] H. Svedhem, D.V. Titov, D. McCoy, J.-P. Lebreton, S. Barabash, J.-L. Bertaux, P. Drossart, V. Formisano, B. Häusler, O. Korablev, W.J. Markiewicz, D. Nevejans, M. Pätzold, G. Piccioni, T.L. Zhang, F.W. Taylor, E. Lellouch, D. Koschny, O. Witasse, H. Eggel, M. Warhaut, A. Accomazzo, J. Rodriguez-Canabal, J. Fabrega, T. Schirmann, A. Clochet, and M. Coradini. Venus express—the first european mission to venus. *Planetary and Space Science*, 55(12):1636–1652, 2007. The Planet Venus and the Venus Express Mission, Part 2.

[8] Dmitrij V. Titov, Nikolay I. Ignatiev, Kevin McGouldrick, Valérie Wilquet, and Colin F. Wilson. Clouds and hazes of venus. *Space Science Reviews*, 214(8):126, Nov 2018.

[9] Philipp Tschandl, Noel Codella, Bengü Nisa Akay, Giuseppe Argenziano, Ralph P Braun, Horacio Cabo, David Gutman, Allan Halpern, Brian Helba, Rainer Hofmann-Wellenhof, Aimilios Lallas, Jan Lapins, Caterina Longo, Josep Malvehy, Michael A Marchetti, Ashfaq Marghoob, Scott Menzies, Amanda Oakley, John Paoli, Susana Puig, Christoph Rinner, Cliff Rosendahl, Alon Scope, Christoph Sinz, H Peter Soyer, Luc Thomas, Iris Zalaudek, and Harald Kittler. Comparison of the accuracy of human readers versus machine-learning algorithms for pigmented skin lesion classification: an open, web-based, international, diagnostic study. *The Lancet Oncology*, 20(7):938–947, 2019.

[10] Jiahui Yu, Xin Li, Jing Yu Koh, Han Zhang, Ruoming Pang, James Qin, Alexander Ku, Yuanzhong Xu, Jason Baldridge, and Yonghui Wu. Vector-quantized image modeling with improved VQGAN. In *The Tenth International Conference on Learning Representations (ICLR)*. OpenReview.net, 2022.